Design and Control of a 6-DOF High-Precision Integrated Positioner

Won-jong Kim, *Senior Member, IEEE*, Tiejun Hu, and Nikhil D. Bhat

***Abstract*—This paper presents the design and control of a high-precision 6-degree-of-freedom (6-DOF) multi-dimensional positioner. This high-precision positioning system consists of a novel concentrated-field magnet matrix and a triangular single-moving platen that carries three 3-phase permanent-magnet linear levitation motor armatures. With a combination of six independent force components, the moving platen can generate any 6-DOF motion. Three aerostatic bearings are used to provide the suspension force against gravity for the system. We designed and implemented digital lead-lag controllers running on a digital signal processor (DSP). To improve the dynamic performance in the vertical direction, we implemented a controller in the feedback path as well. Currently, the positioner has a position resolution of 20 nm and position noise of 10 nm rms in *x* and *y* and 100 nm in *z*. The angular resolution around the *x*-, *y*-, and *z*-axes is in sub-micron order. The planar travel range is 160 mm × 160 mm, and the maximum velocity achieved so far is 0.5 m/s with 5-m/s^2 acceleration in the *y*-direction, which is highly suitable for semiconductor manufacturing applications. Several 2-dimensional motion profiles are presented to demonstrate the stage's capability of accurately tracking any extended planar paths.**

I. Introduction

MANY traditional mechanical stages for *x*-*y* positioning have either crossed-axis-type or gantry-type configurations [1–3]. In wafer steppers in semiconductor manufacturing, the *x*-axis linear stage is typically driven by another *y*-axis stage moving orthogonally to the *x*-axis. The mechanical-bearing tolerance for these precision position control systems should be very small, so they are expensive to make. Some systems use a piezoelectric fine-motion stage on top of a coarse *x*-*y* mechanical stage. The vertical (in the *z*-axis) motions for focusing are generated by additional independent mechanical means. Such systems are complicated and expensive and have complex dynamics, which limits high-speed operation.

The industry has come to use planar motors for two-dimensional positioning applications more frequently than ever. The sawyer motor is one of the earliest inventions in this category [4]. The Sawyer motor is a variable-reluctance type and has frequently been used without explicit position feedback. Its reported step resolution is on the order of 250 μm. Since its primary application was *x*-*y* plotters, this relatively low resolution was sufficient. For precision motion control with a particular emphasis on wafer stepper stages, Hinds and Nocito [5], and Pelta [6] improved the original version of the Sawyer motor. Sawyer-motor-based positioners are prone to large cogging force and excessive attraction force between the mover and the stator. Also as its motion is tightly constrained to a plane, a Sawyer motor cannot provide focus range or local leveling without using fine-motion actuators. Keeping pace with the advance of permanent-magnet material in the last decades, planar motor structures using permanent magnets are presented by Asakawa [7] and Ebihara and Watada [8]. Another planar motion system, which led to the SVGL Micrascan system, is by Buckley, et al. [9].

There are significant advantages of a single levitated moving part in the application of traveling over relatively large planar and small rotational displacements. The multi-dimensional positioner presented in this paper can generate all required fine and coarse motions with only one levitated moving part, and has potential to satisfy the dynamic performance specifications necessary for next-generation deep-submicron microelectronics manufacturing equipment. Fig. 1 shows the picture of the fabricated multi-dimensional positioning system. It has following advantages: (1) It requires no lubricants, does not generate wear particles, is non-contaminating, and thus is highly suited for clean-room environments; (2) One moving part can be designed to have high natural frequencies compared to multi-element stages, which have more complex dynamics; and (3) By eliminating complex mechanical elements the fabrication cost is reduced and the reliability is increased.

A general design method and working principle are provided in this paper. In the later part of this paper, preliminary experimental data and real-time control results are presented.

Manuscript received on September 22, 2003; This work was supported by Texas Advanced Technology Program under Grant No. 000512-0225-2001.

W.-J. Kim and T. Hu are with the Department of Mechanical Engineering, Texas A&M University, College Station, TX 77843-3123, USA (phone: 979-845-3645; fax: 979-845-3801; e-mail: wjkim@mengr.tamu.edu and htjj@tamu.edu).

N. D. Bhat was with the Mechanical Engineering Department, Texas A&M University, College Station, TX 77843-3123, USA. He is now with Pathway Technologies Inc, MI 48152, USA. (e-mail: nikhilbhat@pathwaytechnologies.net).

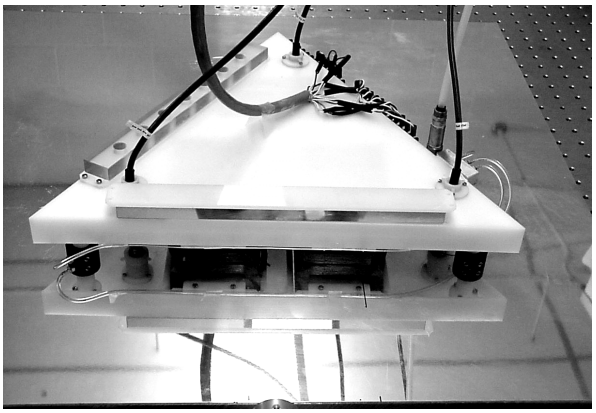

Fig. 1: Picture of the multi-dimensional positioner. The triangular platen is placed on top of a mirror-finished aluminum plate. Beneath the aluminum plate is the concentrated-field magnet matrix.

II. Concentrated-field Magnet matrix

The actuators for this multi-dimensional positioner are three-phase surface-wound linear motors. Error motions due to cogging and nonlinear effects are expected to be minimal [10]. The linear motor uses a novel magnet matrix based on Halbach magnet arrays for its power efficiency and low field distortion [11–12].

The magnet matrix can be constructed by superimposing two orthogonal Halbach magnet arrays [13–14]. The Halbach array has a stronger fundamental field by the factor of $\sqrt{2}$ [11]. By using such an array we can achieve higher power efficiency than those which utilize more conventional magnetization patterns. Using the superimposed Halbach magnet matrix, the levitator design also yields the most compact platen. As shown in Fig. 2, magnet blocks with an arrow have $1/\sqrt{2}$ remanence of the magnets noted with North (N) and South (S) poles. The number of pitches on the magnet matrix decides the travel range of the positioner. In our current design, the magnet matrix was designed to have 6 pitches in both the *x*- and *y*-directions.

The magnet matrix used herein has two kinds of magnets. One is a strong magnet with a remanence of 1.43 T with face-to-face magnetization. The other magnet is a weak magnet with a remanence of 1.10 T with diagonal magnetization. Both the weak and strong magnets are of 12.7 × 12.7 × 12.7 mm with the dimensional tolerance of ±0.05 mm. The magnet matrix consists of a total of 432 weak magnets, 72 strong magnets, and 72 aluminum spacers. The aluminum base plate has the dimension of 609.6 × 609.6 × 38.1 mm.

III. Moving Platen And Linear Levitation Motor

Fig. 3 presents top and bottom perspective views of the moving platen of the multi-dimensional motion generator.

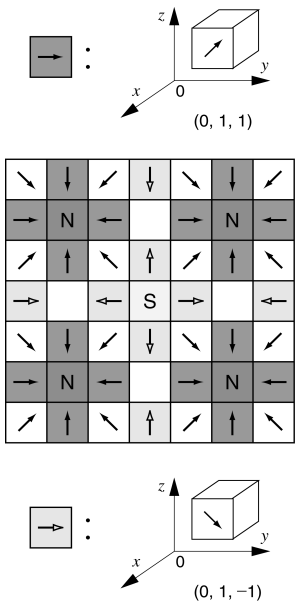

Fig. 2: Concentrated-field magnet matrix

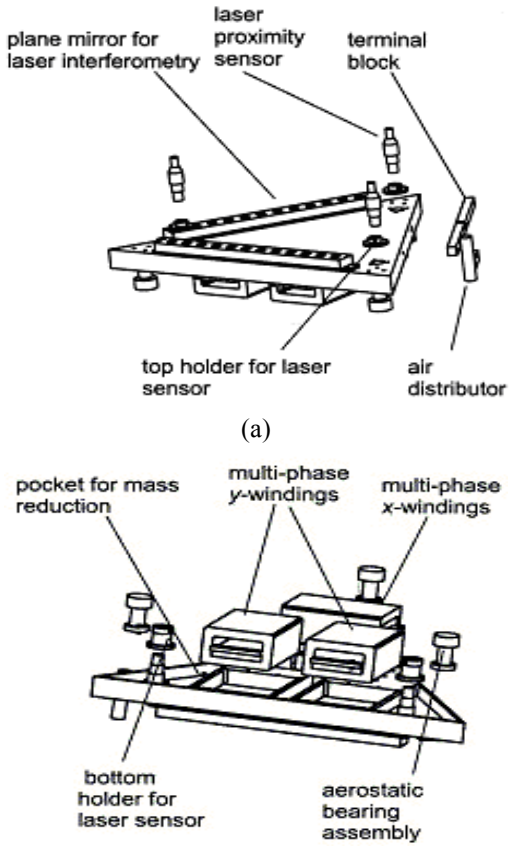

Fig. 3: Perspective views of the single-moving platen. The platen carries the mirrors for the horizontal metrology, and the laser distance sensors for the vertical metrology. It carries three sets of independent multi-phase windings that can generate independent 6-axis vertical and horizontal forces to avoid over-constraint. (a) Top view. (b) Bottom view.

The platen was designed in a triangular shape for compactness. Three linear motor windings, three aerostatic bearings, three laser displacement sensors, two plane mirrors, an air distributor, and terminal blocks are mounted on this platen. On the bottom side of the platen, three pockets were made to mount the linear motor windings. Stick mirrors are mounted on top of the platen for three-axis laser interferometry for horizontal position feedback. Position information in the other three DOFs is obtained through the laser distance sensors.

As shown in Fig. 4, motors *A* and *B* generate the *y*-direction force F_{Ay} and F_{By} to give the *y*- direction motion; and motor *C* generates the *x*-direction force F_{Cx} to give the *x*-direction motion. Each of the three motors can generate the *z*-direction force to give the motion in the *z*-direction and rotations about the *x*- and *y*-axes [12]. Thus all the 6-DOF motions can be generated by these three levitation motors with the force arrangements denoted in Table 1.

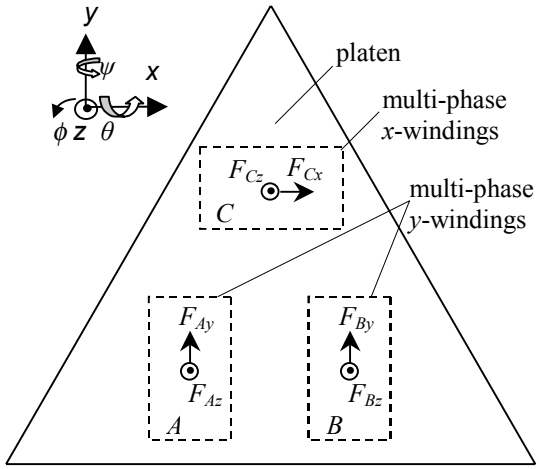

Fig. 4: Definition of the individual force components generated by motors *A*, *B*, and *C*.

TABLE 1. 6-DOF motions generated by the linear motors

	Motor *A*	Motor *B*	Motor *C*
x	$-F_{Ay}$	F_{By}	F_{Cx}
y	F_{Ay}	F_{By}	0
z	F_{Az}	F_{Bz}	F_{Cz}
ϕ	$-F_{Ay}$	F_{By}	0
θ	$-F_{Az}$	$-F_{Bz}$	F_{Cz}
ψ	F_{Az}	$-F_{Bz}$	0

IV. Working Principle And Force Equation

This multi-dimensional positioner works on a two-dimensional superimposed concentrated-field magnet matrix. It carries three sets of windings on its bottom. When currents flow in the multi-phase *x*- and *y*-windings shown in Fig. 2, they generate air-gap magnetic field traveling in the *x*- and *y*-directions, respectively. Consequently, the *x*- and *y*-winding currents interact only with the corresponding *x*- and *y*-magnet array component.

We developed a theoretical framework to determine the resulting force. For preliminary force capability estimation, we chose the following parameters for the integrated positioner. The size of the magnet matrix is 304.8 × 304.8 mm; and the air gap between the magnet matrix and the windings is z_0 = 2.324 mm. The actuator pitch is l = 50.8 mm. The magnet matrix thickness is $\Delta = l/4$ and the winding thickness is $\Gamma = l/5$, determined via a power optimal design. With these parameters, we calculate the driving force for an integrated multidimensional positioner of 22.9 N per motor with 2×10^6-A/m^2 peak current density [12].

The force generated by one pitch of the levitation motor is given by the following equation [14]:

$$\begin{bmatrix} f_y \\ f_z \end{bmatrix} = \frac{1}{2}\mu_0 M_0 \eta_0 N_m G e^{-\gamma_1 z_0} \begin{bmatrix} \cos\gamma_1 y_0 & \sin\gamma_1 y_0 \\ -\sin\gamma_1 y_0 & \cos\gamma_1 y_0 \end{bmatrix} \begin{bmatrix} i_a \\ i_b \end{bmatrix}, \quad (1)$$

where f_y and f_z are the *y*-directed and *z*-directed forces, respectively. The constant

$$G = \frac{\sqrt{2} w l^2}{\pi^2}\left(1 - e^{-\gamma_1 \Gamma}\right)\left(1 - e^{-\gamma_1 \Delta}\right) \quad (2)$$

contains the effects of the motor geometry and is equal to 1.072 × 10^{-5} m^3. The variable y_0 represents horizontal relative displacements of the motors *A* and *B* with respect to the origin. Here i_a and i_b are the peak current components. By continuously changing the value of i_a and i_b, we can control the force in lateral and vertical direction in real time. The parameters have the following values: magnet remanence, $\mu_0 M_0$ = 0.71 T, the winding turn density, η_0 = 3.5246 × 10^6 turns/m^2, effective spatial period N_m = 2, and absolute value of fundamental wave number $\gamma_1 = 2\pi/l$ = 123.25 m^{-1}. The same force equations are valid for motor *C* with replacing y_0 with x_0. The total mass of the platen was measured to be 5.91 kg. This corresponds to a weight of 58 N, while the total vertical force that would be generated by the 3 motors is 68.6 N. Therefore, it is possible to levitate the platen fully magnetically without any modifications in the design.

V. Dynamic Modeling And Control System Design

The mass of the platen was measured as 5.91 kg and the calculated inertia matrix, taken at the platen center of mass, was

$$I = \begin{bmatrix} I_{xx} & -I_{xy} & -I_{xz} \\ -I_{yx} & I_{yy} & -I_{yz} \\ -I_{zx} & -I_{zy} & I_{zz} \end{bmatrix} = \begin{bmatrix} 0.0357 & -0.00120 & -0.000808 \\ -0.00120 & 0.0261 & 0.000263 \\ -0.000808 & 0.000263 & 0.0561 \end{bmatrix} \quad (3)$$

in kg-m^2. As the products of inertia are less than 5% of the principal moments of inertia, we neglect them in the present dynamic model.

Although it is possible to levitate the positioner magnetically, we use three aerostatic bearings to provide the suspension force to the system, which will significantly reduce the power consumption of the system. As a result,

the platen is modeled as a pure mass without friction, for the translation in the *x*- and *y*-directions. The dynamics of this pure mass model is presented by the Newton's equation of motion

$$M\frac{d^2x}{dt^2} = f_x \tag{4}$$

$$M\frac{d^2y}{dt^2} = f_y, \tag{5}$$

where M is equal to 5.91 kg and $f_{(x,y)}$ is the magnetic modal forces generated by motors *A*, *B*, and *C*.

For the control of rotation around the *z*-axis, the dynamics of the system is represented by the following differential equation:

$$I_{zz}\frac{d^2\phi}{dt^2} = \tau_z, \tag{6}$$

where τ_z is the torque from the magnetic origin about the *z*-axis, and I_{zz} is the principal moment of inertia about the *z*-axis.

The platen is modeled as a spring-mass system in the *z*-direction because of the existence of the three aerostatic bearings:

$$M\frac{d^2z}{dt^2} + K_z z = f_z, \tag{7}$$

where K_z is the effective spring constant of the aerostatic bearings and f_z is the vertical direction force generated by the three motors. By experiments based on the Hooke's law, K_z was measured as 10^6 N/m.

Because the three air bearings can be regarded as three springs, it can be expected the dynamics in the rotation around the *x*- and *y*-axes can also be modeled as a spring-mass system:

$$I_{xx}\frac{d^2\theta}{dt^2} + K_\theta\theta = \tau_\theta \tag{8}$$

$$I_{yy}\frac{d^2\psi}{dt^2} + K_\psi\psi = \tau_\psi, \tag{9}$$

where τ_θ and τ_ψ are the torque around the *x*- and *y*-axes respectively, and K_θ and K_ψ are also the effective torsional spring constants with regard to the *x*- and *y*-axes, which were determined as 10^4 N·m/rad by experiments.

Sensor measurements are sent to the DSP, and the digital controller implemented on the DSP controls the platen in all 6 DOFs. The sampling rate of this control system is 5 kHz. Two similar digital lead-lag controllers for translation in the *x*- and *y*-directions were designed. The implemented digital lead-lag compensator is

$$G_{x,y}(z) = 740000\left(\frac{z-0.9903}{z-0.7970}\right)\left(\frac{z-0.9979}{z-1}\right). \tag{10}$$

The crossover frequency is 21 Hz, and the phase margin is 57.6°.

A similar digital lead-lag controller is designed to control the rotation around the *z*-axis as the following

$$G_\phi(z) = 13100\left(\frac{z-0.9903}{z-0.7970}\right)\left(\frac{z-0.9979}{z-1}\right). \tag{11}$$

The crossover frequency is 38 Hz, and the phase margin is 62.7º.

From the vertical dynamic model of vertical direction motion, there exists resonance due to the air bearing spring in the system. The resonant frequencies are 65, 84, and 99 Hz in the *z*-, θ-, and ψ-directions respectively. These resonant frequencies will affect the dynamic performance of the system significantly. They may cause the system going unstable or make the system have a slow response. To improve the dynamic performance in vertical direction, we designed a new controller based on the following structure:

The controller $C(s)$ was implemented in the feedback path to reduce the effect of the aerostatic-bearing resonance in the vertical dynamics as shown in Fig. 5. It modifies the original plant so that the system becomes more stable and has a faster step response. The integrator K/s is used to eliminate the steady-state position error. The implemented digital controller $C(z)$ are:

$$C_z(z) = 2.000\times10^6\frac{z-1}{z-0.8187} \tag{12}$$

$$C_{\theta,\psi}(z) = 1.083\times10^4\frac{z-1}{z-0.8465}. \tag{13}$$

VI. Experimental Results

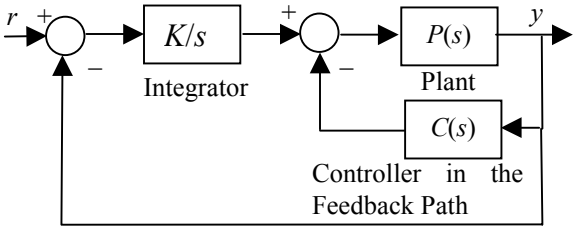

Fig. 5: Control structure in vertical direction control

To test the dynamic performance of the system in all 6 axes, we obtained step responses as shown in Fig. 6. The rise time is less than 3 ms, and the settling time is less than 150 ms without steady-state error in *x* and *y* (Fig. 6 (a) and (b)). The vertical step responses (Fig. 6 (c), (d), and (e)) are a little longer because of the damped dynamics with the three aerostatic bearings. The more oscillatory behavior in the *x*-direction is believed to originate from the fact that motor *C* generates a perturbation torque. Although motors *A* and *B* would compensate for this torque, it might not have been completely canceled due to modeling errors. The low-frequency (at about 10 Hz) disturbance in ϕ is believed to be generated by the umbilical cables and air pipes connected to the platen.

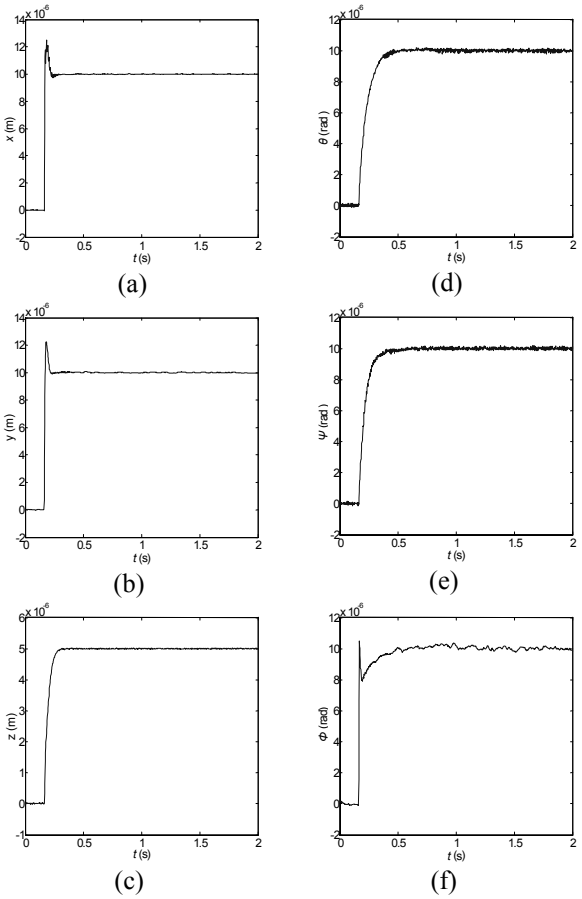

Fig. 6: 10-μm step responses in (a) x and (b) y. (c) 5-μm step response in z. 10-μrad step response in (d) θ, (e) ψ, and (f) ϕ.

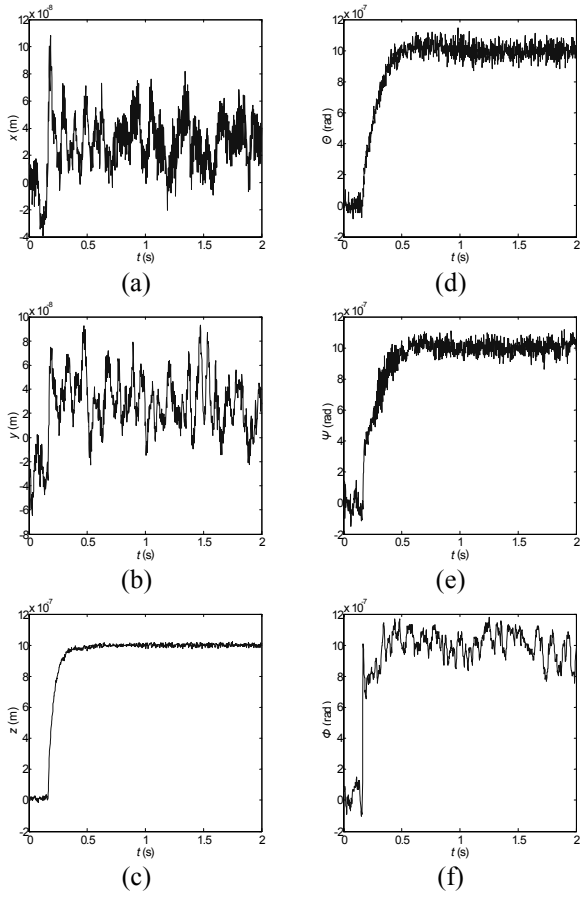

Fig. 7: 30-nm step responses in (a) x and (b) y. (c) 1-μm step response in z. 1-μrad step responses in (d) θ, (e) ψ, and (f) ϕ.

Parts (a) and (b) in Fig. 7 present a 30-nm step response in x and y; part (c) presents a 1-μm step response in z; parts (d), (e), and (f) represent 1-μrad step response in θ, ψ, and ϕ, respectively. There exists a 60-nm peak-to-peak (10 nm rms) position noise in the system. Both the noise generated by the three aerostatic bearings and the external disturbance transmitted through the umbilical cables are believed to contribute to the position noise. With these experimental results, we demonstrated the integrated positoner presented herein possessed the potential to satisfy the requirement of sub-micron semiconductor manufacturing.

This prototype positioner currently has a travel range of 160 mm in both x and y. Fig. 8 shows that the stage moved 160 mm in x and y, respectively. Furthermore, this multidimensional positioner has the capability of following large arbitrary planar paths. Fig. 9 shows that the positioner followed circular and triangular motion trajectories.

The multidimensional positioner presented herein currently is capable of generating maximum velocity of 0.5 m/s with maximum 5-m/s^2 acceleration in the y-direction. Fig. 10 (a) shows the stage moved back and forth with a travel range of 140-mm in the y-direction. The platen first moves in the +y-direction at the maximum acceleration of about ½ g (5 m/s^2). When the velocity reached 0.5 m/s, the platen stopped accelerating and moved at this constant velocity. After 0.18 seconds, the platen started to decelerate at 5 m/s^2 until its velocity reached zero. After resting at the position of 14 cm for a while, the stage moved back to its original position. Fig. 10 (b) shows the corresponding velocity profile.

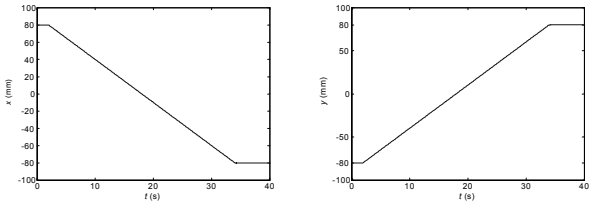

Fig. 8: 160-mm travel range traversed in both (a) x and (b) y.

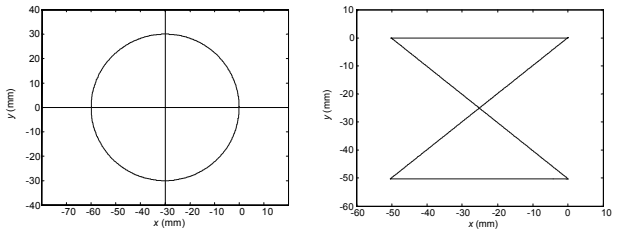

(a) (b)

Fig. 9: Capability of following planar paths in (a) a circle of 6-cm diameter and (b) a double triangle.

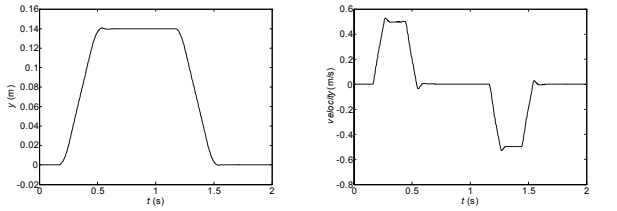

(a) (b)

Fig. 10: (a) Position and (b) velocity profiles in y with 0.5-m/s maximum velocity and 5-m/s^2 maximum acceleration.

VII. Conclusion

A high-precision multi-dimensional positioning system consisting of a novel concentrated-field magnet matrix based on Halbach magnet arrays and a triangular single-moving platen was developed and tested. The actuators for the positioner are three 3-phase linear levitation motors, which exhibit no cogging force. Each of these actuators can generate vertical as well as lateral forces.

After implementing digital feedback controllers, we achieved a position resolution of 20 nm with a position noise of 10-nm rms in both x and y, and submicron resolution in other axes, which can be seen in the step responses presented in the paper. This prototype positioner has a planar travel range of 160 × 160 mm, which can be easily extended. It currently has 0.5-m/s maximum speed at an acceleration of 5 m/s^2 in the y-direction. The large arbitrary planar-motion generation capability of this positioning stage was demonstrated by following motion profiles such as a 6-cm-diameter circle and a double triangle.

VIII. Acknowledgement

This material is based in part upon work supported by the Texas Advanced Technology Program under Grant No. 000512-0225-2001.

References

[1] G. van Engelen and A. G. Bouwer, "Two-step positioning device using Lorentz forces and a static gas bearing," U.S. Patent No. 5 120 034, June 1992.

[2] S. Sakino, E. Osanai, M. Negishi, M. Horikoshi, M. Inoue, and K. Ono, "Movement guiding mechanism," U.S. Patent No. 5 040 431, August 1991.

[3] S. Wittekoek and A. G. Bouwer, "Displacement device, particularly for the photolithographic treament of a substrate," U.S. Patent No. 4 655 594, April 1987.

[4] B. A. Sawyer, "Magnetic positioning device," U.S. Patent No. 3 376 578, April 1987.

[5] W. E. Hinds and B. Nocito, "The Sawyer linear motor," *Proceedings of The Second Symposium on Incremental Motion Control Systems and Devices*, pp. W-1–W-10, 1973.

[6] E. R. Pelta, "Two Axis Sawyer Motor," *Proceedings of the 12th Annual IEEE Industrial Electronics Society Conference*, pp. 3–8, 1986.

[7] T. Asakawa, "Two dimensional precise positioning devices for use in a semiconductor apparatus," U.S. Patent No. 4 535 278, August 1985.

[8] D. Ebihara and M. Watada, "Study of a basic structure of surface actuator," *IEEE Transactions on Magnetics*, vol. 25, no. 5, pp. 3916–3918, 1989.

[9] J. D. Buckley and D. N. Galburt, and C. Karatzas, "Step-and-scan lithography using reduction optics," *Journal of Vacuum Science and Technology*, B, vol. 7, no. 6, pp. 1607–1612, 1989.

[10] W.-J. Kim and D. L. Trumper, "Force ripple in surface-wound permanent- magnet linear motors," *Proc. IEEE Int. Magnetics Conf.*, FE-03, April 1996.

[11] K. Halbach, "Design of permanent multipole magnets with oriented rare earch cobalt material." *Nucl. Instrum. Methods*, vol. 169, no. 1, pp. 1–10, 1980.

[12] D. L. Trumper, W.-J. Kim, and M. E. Williams, "Design and analysis framework for permanent-magnet machines," *IEEE Transactions on Industry Applications*, vol. 32, no. 2, pp. 371–379, March/April 1996.

[13] D. L. Trumper, W.-J. Kim, and M. E. Williams, "Magnetic arrays," U.S. Patent Office, Patent No. 5 631 618, May 1997.

[14] W.-J. Kim, *High-precision Planar Magnetic Levitation*, Doctoral Thesis, Massachusetts Institute of Technology, June 1997.